REPORT DOCUMENTATION PAGE

AFRL-SR-AR-TR-04-

0521

1. REPORT DATE *(DD-MM-YYYY)*
09-2004

2. REPORT TYPE
Final Report

3. DATES COVERED *(From - To)*
01 Apr 02 - 31 Dec 03

4. TITLE AND SUBTITLE
Friction Test Specimens That WIll Be Used to Measure Nonlinear Damping and Stiffness

5a. CONTRACT NUMBER

5b. GRANT NUMBER
F49620-02-1-0168

5c. PROGRAM ELEMENT NUMBER

5d. PROJECT NUMBER

5e. TASK NUMBER

5f. WORK UNIT NUMBER

6. AUTHOR(S)
Jerry H. Griffin

7. PERFORMING ORGANIZATION NAME(S) AND ADDRESS(ES)
Department of Mechanical Engineering
Carnegie Mellon University
Pittsburgh PA 15213

8. PERFORMING ORGANIZATION REPORT NUMBER

9. SPONSORING/MONITORING AGENCY NAME(S) AND ADDRESS(ES)
USAF/AFRL
AFOSR
801 N. Randolph Street
Arlington VA 222003

NA

10. SPONSOR/MONITOR'S ACRONYM(S)
AFOSR

11. SPONSOR/MONITOR'S REPORT NUMBER(S)

12. DISTRIBUTION/AVAILABILITY STATEMENT

Distribution Statement A. Approved for public release; distribution is unlimited.

20041028 033

13. SUPPLEMENTARY NOTES

14. ABSTRACT
The funds received from the AFOSR were to be used to 1) purchase materials and machine friction test specimens and 2) refurbish a Brown and Sharpe Coordinate Measurement Machine (CMM). The specimens were used in an initially Carnegie Mellon University (CMU) supported and then US Navy supported research project titled, "Physical Models of Friction Constraint and The Effect of Friction on Bladed Disk Dynamics." For the first year, the graduate student working on the project was supported by CMU as a Teaching Assistant. The AFOSR funds allowed us to make specimens and begin testing before we started getting Navy funding. The CMM machine allowed us to check the dimensions of the specimens that we had manufactured and characterize how wear affected the contact geometry.

15. SUBJECT TERMS

16. SECURITY CLASSIFICATION OF: a. REPORT	b. ABSTRACT	c. THIS PAGE	17. LIMITATION OF ABSTRACT	18. NUMBER OF PAGES	19a. NAME OF RESPONSIBLE PERSON
U	U	U	UU	16	19b. TELEPHONE NUMBER *(Include area code)*

BEST AVAILABLE COPY

RECEIVED SEP 27 2004

Friction Test Specimens That Will Be Used to Measure Nonlinear Damping and Stiffness

FINAL PERFORMANCE REPORT

AWARD NO. F49620-02-1-0168
AWARD DATE: 1 APRIL 2002

PROJECT ENGINEER: CAPTAIN C. ALLRED
AFOSR

BY

J. H. GRIFFIN
DEPARTMENT OF MECHANICAL ENGINEERING
CARNEGIE MELLON UNIVERSITY
PITTSBURGH, PA 15213
[PHONE NO. (412) 268-3860]

SEPTEMBER 2004

1. INTRODUCTION

The funds received from the AFOSR were to be used to 1) purchase materials and machine friction test specimens and 2) refurbish a Brown and Sharpe Coordinate Measurement Machine (CMM). The specimens were used in an initially Carnegie Mellon University (CMU) supported and then US Navy supported research project titled, "Physical Models Of Friction Constraint And The Effect Of Friction On Bladed Disk Dynamics." For the first year, the graduate student working on the project was supported by CMU as a Teaching Assistant. The AFOSR funds allowed us to make specimens and begin testing before we started getting Navy funding. The CMM machine allowed us to check the dimensions of the specimens that we had manufactured and characterize how wear affected the contact geometry. Additional, details are provided below.

2. TEST SPECIMENS AND EQUIPMENT PURCHASED

2.1 Test Specimens

Approximately $15,000 of the AFOSR funds were used to manufacture test specimens used to measure cyclic response. The geometry of the test specimens were similar to that of under-platform friction blade dampers used in the hot section of gas turbines. We made specimens with two types of geometries. One type had spherical heads and the other flat, cylindrical heads (Figure 1). The damper specimens fit inside "fork specimens," an example of which is shown in Figure 2. The specimens were then put into an MTS machine. The fork was attached to the top actuator in the MTS machine and the damper specimen to the bottom actuator. A clamp was then applied across the fork that produced a compressive load on the outside of the fork that was transmitted to the damper specimen (see Figure 3). Thus, the damper and fork specimens were connected through a friction interface.

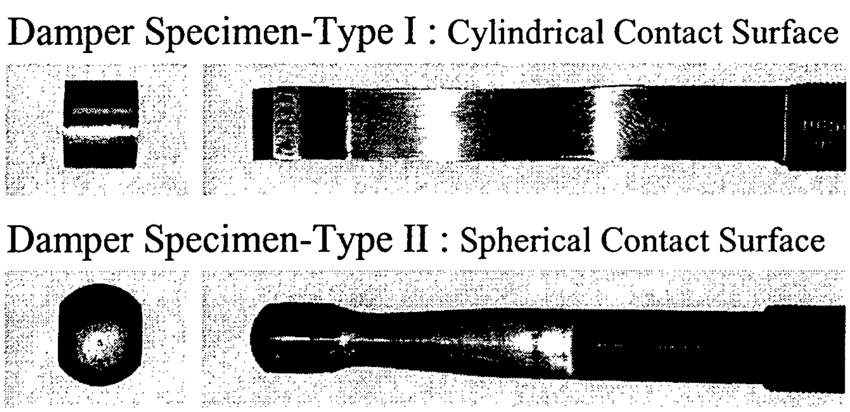

Figure 1 Photographs of Internal Damper Specimens: Top photos – Flat Cylinder, Bottom photos - Spherical

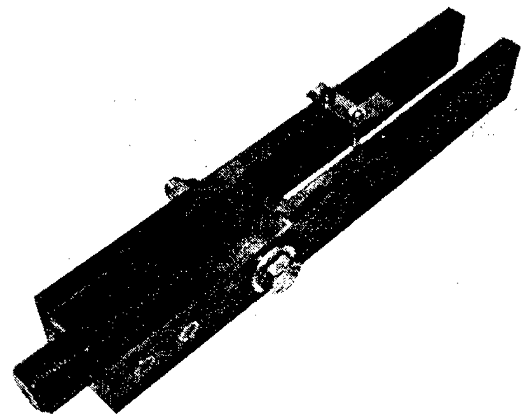

Figure 2 Photograph of Outside, Fork Specimen

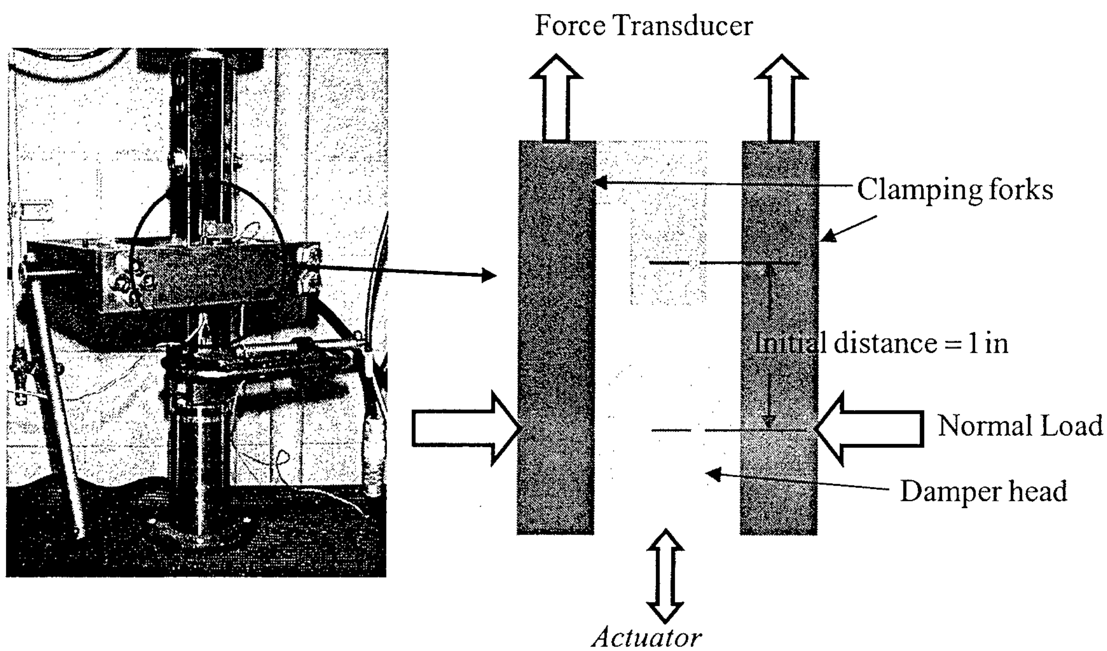

Figure 3 Left Photo Shows Clamp and MTS Machine. Right Schematic Explains the Arrangement of the Test Pieces

The normal load on the contact surfaces was measured using a strain gage mounted at the center of the damper specimen. A sinusoidally varying force was applied in the vertical direction to the frictionally constrained system that caused the friction interface between the fork and the damper to slip. The MTS test system plotted the resulting displacement as a function of the applied load. Typical sets of hysteresis curves are shown in Figure 4 for a range of amplitudes of input forces. The figures on the left are for a normal load (from the clamp) of 2000 lbf and the ones on the right for a normal load of 4000 lbf.

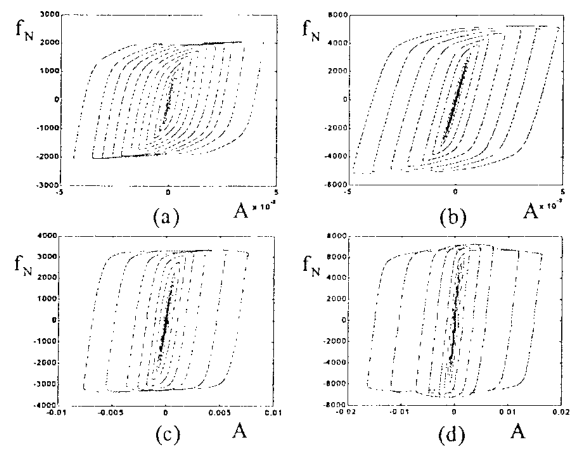

Figure 4 Hysteresis Curves: (a) and (b) are for the flat, cylindrical specimen. (c) and (d) for the spherical specimen

Tests were conducted with the specimens over a range of normal loads and amplitudes. The data was processed and compared with theoretically predicted results. The agreement between the theory and the experimental results was good. A detail discussion of the testing and analysis was presented as a paper at the ASME Turbo Expo 2004 Power for Land, Sea, and Air in Vienna, Austria in June 2004. A copy of the paper is attached as an Appendix. The paper has also been accepted for publication in the ASME Journal of Engineering for Gas Turbines and Power.

2.2 CMM Machine

AFOSR funds were also used to refurbish a Brown and Sharpe CMM machine, Figure 4. The CMM machine was used throughout the project to check the dimensions of test specimens as initially manufactured and also to characterize geometry changes caused by wear. We received approval from the AFOSR project engineer, Dr. D. Mook, to use the funds for the purpose.

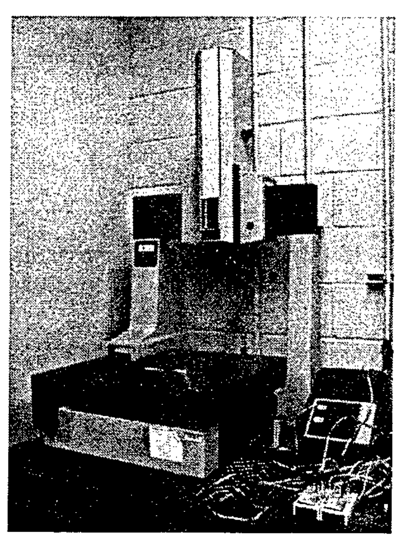

Figure 4 Refurbished CMM Machine

3. FOLLOW-ON RESEARCH

The quasi-static testing and analysis that we did using the AFOSR test specimens showed that friction contact could be predicted from first principles using nonlinear contact mechanics. We have subsequently performed vibration tests on turbine blade-like specimens to show that the quasi-static results apply to vibrating under-platform dampers. Photographs of the test apparatus and the under-platform damper (with spherical heads) are shown in Figure 5.

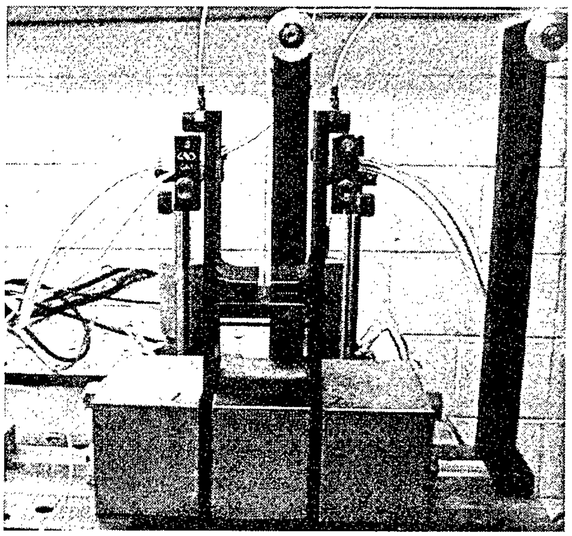

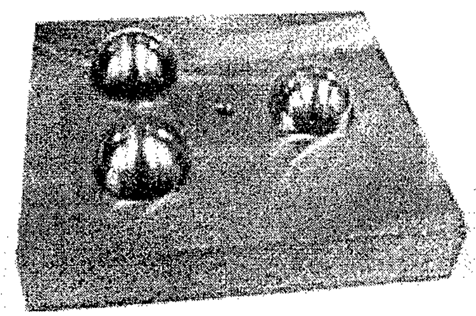

Figure 5 Vibration Test Apparatus and Under-Platform Damper Specimen

The performance of the damper is depicted in Figure 6. In this figure, the peak vibratory amplitude of the blade tip is plotted as a function of the magnitude of the excitation force. The curve is nonlinear since friction effects are nonlinear. The experimental data agree very well with analytical predictions indicated by the continuous curve. The analytical prediction were based on the theory developed using the quasi-static test results discussed in Section 2. Consequently, this follow-on research has shown that damper performance can, in fact, be predicted from first principles using nonlinear contact mechanics.

The research of the student who performed these studies, Mr. Kyun Hee Koh, is currently being documented in his PhD theses. The more recent results on the vibration tests were just completed this summer and were presented by Mr. Koh at the GUIde Consortium annual meeting, July 2004, in Pittsburgh, PA.

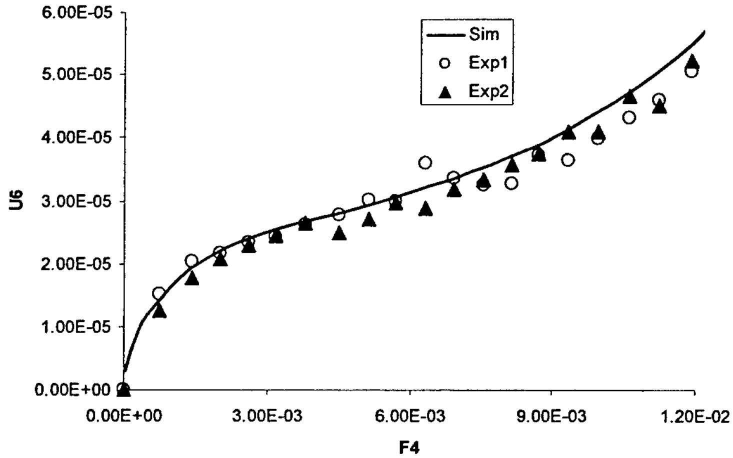

Figure 6 Damper Performance Curve Compares Prediction with Measured Data

ATTACHMENT 1

Relevant Publication

Proceedings of ASME Turbo Expo 2004
Power for Land, Sea, and Air
June 14-17, 2004, Vienna, Austria

GT2004-53278

CHARACTERIZATION OF TURBINE BLADE FRICTION DAMPERS

K-H. Koh
Carnegie Mellon University

J.H. Griffin
Carnegie Mellon University

S. Filippi[1]
Carnegie Mellon University

A. Akay
Carnegie Mellon University

ABSTRACT

This paper discusses an approach for characterizing the dynamic behavior of a friction damper. To accomplish this, the deflection of the damper is measured as a function of an applied force for a range of amplitudes, normal loads, and excitation frequencies. The resulting hysteresis curves are used to generate curves of nonlinear stiffness and damping as a function of the amplitude of motion. A method of presenting this information in a dimensionless format is demonstrated. This format allows direct comparisons of the nonlinear stiffness and damping of actual dampers with that often used in analytical models to compute the dynamic response of frictionally damped turbine blades. It is shown that for the case of a damper with a spherical head significant differences exist between the actual behavior of the damper and that often assumed in simple analytical models.

In addition, Mindlin's analysis of a sphere on a half space is used to estimate the damper's stiffness as well as its theoretical hysteresis curves. The hysteresis curves are then used to determine dimensionless stiffness and damping curves. The results compare favorably with those found experimentally.

INTRODUCTION

Friction dampers are used in gas turbine engines to increase energy dissipation and reduce vibratory response. Dampers are pieces of metal that fit between the blades and that are held in place by centrifugal force. They dissipate energy when sliding occurs across the friction interface. In addition, the damper acts like a weak nonlinear spring that affects the frequency of peak, vibratory response. Thus, friction dampers control the amplitude and, less strongly, the frequency of the peak response.

Two recent review papers on the general topic of friction damping are by Feeny et al. [1] and by Gaul and Nitsche [2]. Predicting and optimizing the performance of turbine blade friction dampers is an active area of research in its own right. For examples consider the review paper by Griffin [3], the papers by Yang and Menq [4, 5, 6, 7], Sanliturk et al. [8], Petrov and Ewins [9, 10], Szwedowicz et al. [11], Cha and Sinha [12, 13], Csaba [14], and Sextro et al. [15]. Computer codes that developed from these research efforts are widely used by the gas turbine industry to predict and optimize damper performance. Nearly all of the codes use spring elements that can slip as their basic friction element [16]. For example a friction damper that connects adjoining blade platforms may be modeled by a spring connection (or a series of spring connections in parallel) that slips if the magnitude of its force equals a certain limiting value, μN. Analyzing the effect of the friction force becomes more complex when the damper and blade's contact surfaces are inclined so that the normal load varies dynamically during a cycle [17, 18] or if the relative motion across the contacting surfaces follows a two dimensional path [19, 20].

A significant effort has been made by engine manufacturers to assess how well the resulting computer codes predict damper behavior. Recently, the US Air Force Office of Scientific Research, the US Navy, and the Sandia National Laboratories sponsored two workshops on contact mechanics and friction damping [21]. It was attended by representatives from General Electric, Pratt & Whitney, Rolls Royce, and Siemens Westinghouse as well as representatives from academia and US government. The general opinion expressed by the industrial representatives at the workshop was that the codes used by industry have to be calibrated with test data before they can be used to reliably predict the performance of a particular blade/damper design under engine conditions. Specifically, the consensus view was that the damper stiffness used in the computer code that correlates with the test data is usually significantly less than that calculated from a finite

[1]On leave from Politecnico di Torino, Turin, Italy.

element model of the damper. The purpose of the research reported in this paper is to measure the properties of a real, but simple, damper and to assess why it might be difficult to characterize its behavior with a simple spring element.

In order to perform this assessment, a prototype damper with a spherical head was manufactured and tested under various conditions. The data from the resulting friction force - displacement hysteresis curves were processed to determine the damper's effective nonlinear damping and stiffness as a function of the amplitude of the motion across the friction interface. The results were then compared with that of the simple spring damper model and were seen to exhibit significant differences.

The contact problem of a sphere on a half space subjected to periodically applied shear loads was analyzed by Mindlin [22, 23] and by Deresiewicz [24]. Experimental studies that support the theory have been reported by Mindlin [25], Johnson [26], and Goodman and Brown [27]. The hysteresis curves of damper with a spherical head in contact with a flat plate can be predicted analytically using Mindlin's analysis. The resulting curves can then be processed in the same manner as the experimental data to predict the damper's effective nonlinear damping and stiffness. It will be shown that Mindlin's solution accurately captures the experimental behavior of the damper over a range of testing conditions.

The organization of this paper is as follows. First, the analytical properties of the spring damper element are reviewed. They will be used as the benchmark in this study. Of specific interest is the manner in which the dimensionless, nonlinear stiffness and damping curves are used to characterize its behavior. Section 3, will describe how the hysteresis curves of the test dampers are measured and then processed to get dimensionless, nonlinear stiffness and damping curves that can be compared with those of the spring damper. In Section 4, Mindlin's solution will be used to generate theoretical values of nonlinear stiffness and damping that are then compared with the experimental results. Implications of the results are discussed in Section 5. Concluding remarks are provided in the last section.

1. SPRING DAMPER MODEL: BENCHMARK

To understand how friction dampers work, consider the case of a single degree of freedom oscillator constrained by the spring friction damper shown in Figure 1. For a spring damper the energy dissipated during one cycle of motion is the area enclosed by the bilinear hysteresis curve shown in Figure 2. It is considered a "macroslip" element since it does not dissipate any energy unless there is gross slip across the interface. It is characterized by its stiffness, k_d, and the slip load, N.

If the nonlinear friction force from the spring damper that resists the motion is f_N, the equation of motion is

$$m\ddot{x} + c\dot{x} + kx = f_0 \cos \omega t - f_N(t) \qquad (1)$$

The nonlinear friction force may be approximated by a spring and viscous damper acting in parallel, i.e.,

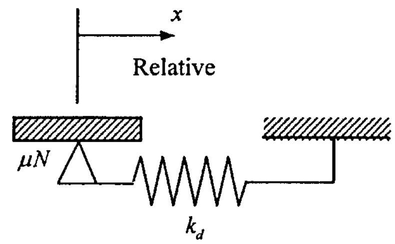

Figure 1: Spring damper element

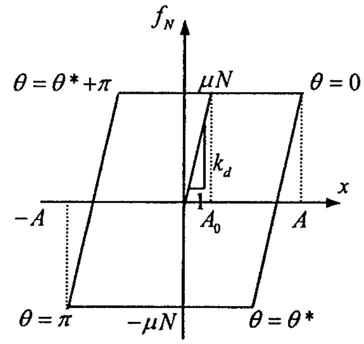

Figure 2: Hysteresis from spring damper element

$$f_N(t) \approx k_e x + c_e \dot{x} \qquad (2)$$

The effective stiffness and damping are found using the Harmonic Balance (HB) method. Some examples of the application of HB method can be found in [16, 28, 29, 30]. In the HB method it is assumed that the displacement is sinusoidal and that the nonlinear force has the same period as the motion. The force is expanded in a Fourier series and truncated after its fundamental terms since the mass spring system is an oscillator that filters out the higher frequency components. The fundamental terms in the Fourier series can be expressed so that one is in-phase with the motion and one is out-of-phase. The in-phase term effectively represents a spring force and the out-of-phase term an equivalent damping force. Since the Fourier coefficients depend on the amplitude of the motion, the effective stiffness and damping are nonlinear functions of the amplitude. The amplitude of the motion can be normalized by dividing by the distance required to cause slip, i.e., $\tilde{A} = A/(\mu N / k_d)$. Then the non-dimensionalized effective stiffness and damping of the spring friction element are given by the equations[31]:

$$\tilde{k}_e(\tilde{A}) = \frac{k_e(A)}{k_d} = \frac{1}{\pi}\left[\cos^{-1}\left(1-\frac{2}{\tilde{A}}\right) - 0.5\sin\left\{2\cos^{-1}\left(1-\frac{2}{\tilde{A}}\right)\right\}\right] \qquad (3)$$

$$\tilde{c}_e(\tilde{A}) = \frac{c_e(A)}{k_d/\pi\omega} = \frac{4}{\tilde{A}}\left(1-\frac{1}{\tilde{A}}\right) \qquad (4)$$

where the arc cosine is defined to lie between 0 and π. The dimensionless stiffness and damping of a spring friction element are plotted as a function of amplitude in Figures 3 and 4. They completely characterize the dynamic behavior of the spring damper and determine the response of the single degree of freedom system. Note, that for $A < 1$, the damper does not slip. Consequently, the damper's effective stiffness remains equal to its elastic value and its effective damping is zero, i.e., the spring element exhibits only macroslip behavior.

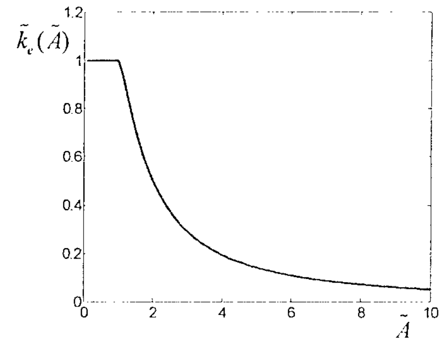

Figure 3: Nondimensionalized effective stiffness

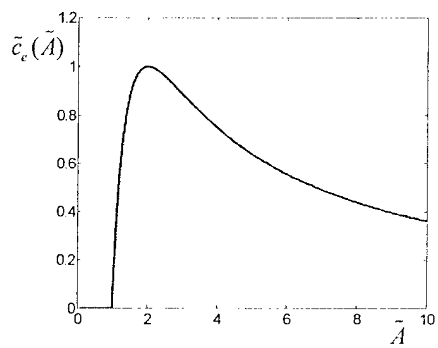

Figure 4: Nondimensionalized effective damping

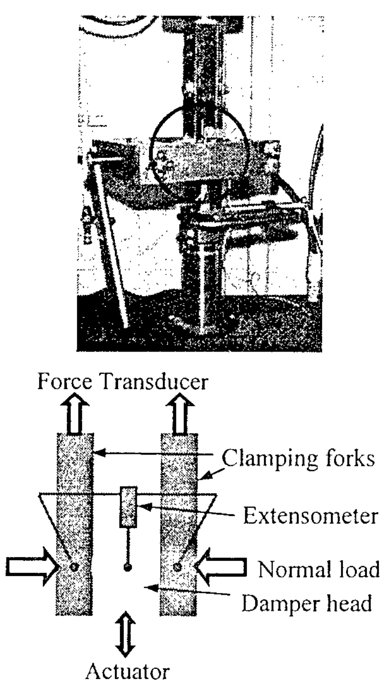

Figure 5: Experimental setup for quasi-static test

2. EXPERIMENT

2.1 Experimental setup

Two different experiments are used to measure the behavior of the dampers. One is a quasi-static test conducted at 0.1 Hertz. The second is a dynamic test conducted at 50 Hertz. They are described in the following sub-sections.

Quasi-static test. The quasi-static tests were done using the MTS testing machine shown in Figure 5. The specimens have two parts. A fork type specimen with two prongs is mounted in the upper part of the MTS and damper type specimen, Figure 6, in the lower part. The friction damper specimen is inserted between the prongs which are then compressed with a clamp. The prongs of fork are thin plates that are meant to represent the blade's platform. Strain gages are attached to the flat faces of the damper specimen. They are used to monitor the normal load on the friction interface during the tests. An extensometer is used to measure the relative displacement. A special fixture was designed so that the extensometer measures the relative displacement directly across the friction interface. This eliminates errors caused by the rotational deflection of the fork and improves the repeatability of the measurement. The load cell in the MTS machine is used to measure the friction force.

In order to facilitate testing, the specimens were made larger than those commonly used in engines. If the dimensions of a damper are scaled by a factor S then the displacements are also scaled by S and are easier to measure. To compensate, the normal loads are scaled in proportion to the square of S in order to maintain realistic contact stresses. The specimens are made of Maraging steel. The advantages of Maraging steel are its fair machinability before heat treating and its high yield stress after. Once it is heat-treated, it has a yield stress of 2,068-2,758 MPa, comparable to that of the super Nickel alloys used in turbines. An advantage of using this high strength alloy is that the deformation in the contact region tends to stay elastic. The faces of the damper that come in contact with the prongs of the fork are spherical and have a radius of curvature of 127 mm.

Dynamic test. The apparatus used in the dynamic test is shown in Figure 7. Its complete description is given in [32]. In this experiment, the horizontal beam element is excited by a shaker at 50 Hertz. A friction damper is attached to the beam at its center. The damper consists of a hemispherical damper specimen in contact with a flat plate. Its radius of curvature is 12.7 mm, an order of magnitude smaller that those tested in the MTS machine. The normal load is applied using pulleys and a dead weight. The normal load was maintained at 69 N during the tests reported here. The damper shear force is measured by a load cell in series with the damper specimen. The relative motion across the friction interface is measured with a laser vibrometer.

Hysteresis curves were generated under dynamic conditions using this apparatus. The tests provide an interesting contrast to the quasi-static experiment since the frequency is two orders of magnitude higher, the radius of curvature one order of magnitude lower, and the normal load two orders of magnitude lower than in the quasi-static tests.

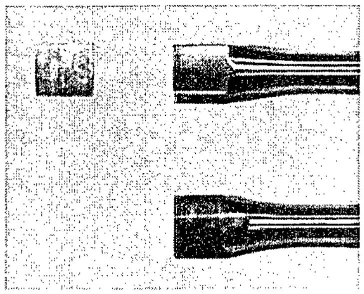

Figure 6: Friction damper specimen for quasi-static test

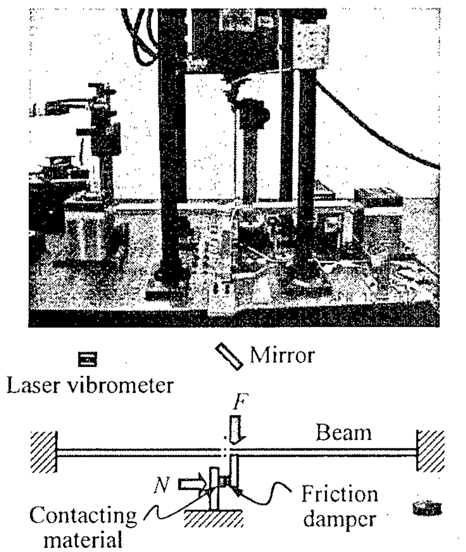

Figure 7: Experimental setup for dynamic test

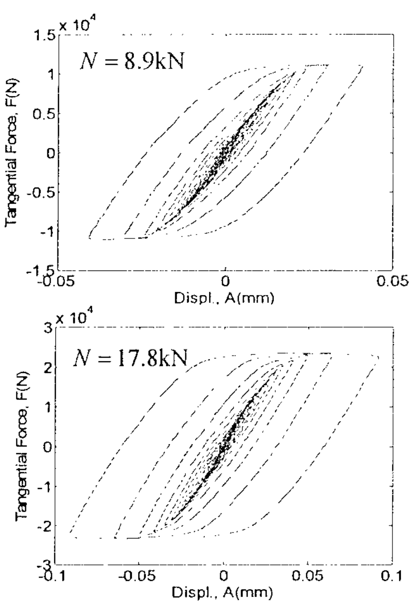

Figure 8: Hysteresis curves from quasi-static tests

2.2 Measurement

The tests were conducted for a range of amplitudes and at different normal loads. Representative results for quasi-static test are shown in Figure 8. The quasi-static tests were done for two different normal loads, 8.9 kN and 17.8 kN. Similar curves were generated using the dynamic test apparatus, Figure 9.

2.3 Data processing

The hysteresis curves from the tests were processed in a manner consistent with that used to determine the equivalent stiffness and damping of the spring damper. First, it was necessary to non-dimensionalize the amplitude of motion. This requires knowing the damper's physical stiffness k_d and the force required for gross slip, μN. The stiffness was inferred from the hysteresis curves by averaging the slopes during the initial unloading and loading portions of the cycle $k_d \approx (k_1 + k_2)/2$, Figure 10. The gross slip load μN was also determined from the hysteresis curves by applying sufficiently large amplitude that the curves flattened out. Thus, the characteristic length $A_0 = \mu N / k_d$ was determined from the experimental data. The dimensionless amplitude $\tilde{A}$ could then be calculated by dividing the physical amplitude by A_0.

The dimensionless effective stiffness and damping are given by:

$$\tilde{k}_e(\tilde{A}) = \frac{1}{\pi \tilde{A} \mu N} \int_0^{2\pi} f_N \cos\theta d\theta \tag{5}$$

$$\tilde{c}_e(\tilde{A}) = -\frac{1}{\tilde{A} \mu N} \int_0^{2\pi} f_N \sin\theta d\theta \tag{6}$$

These quantities were calculated using the force and displacement information from the hysteresis curves and integrating the data numerically in MATLAB. The integration was fairly accurate since a large number of data points, about 200, were measured each cycle.

2.4 Key results

Figure 11 shows the nonlinear effective stiffness and damping plots produced by the quasi-static and dynamic tests. Observe that the quasi-static experiments with the two different normal loads 8.9 kN and 17.8 kN give almost identical curves. The normalized data points from the dynamic test also look quite similar. This is quite an interesting result since it tends to imply that a unique set of dimensionless stiffness and damping curves exist for a particular damper geometry even though the test conditions varied significantly from one test to the next.

When our experimentally determined curves of effective stiffness are compared with those of the spring damper they agree reasonably well for large displacements, $\tilde{A} > 3$. However, because of microslip the dimensionless effective stiffness of the experimental damper is smaller than that of the spring damper when the amplitude is small. More importantly, the experimental data has much more damping at low amplitudes than the spring model and somewhat less at high amplitudes.

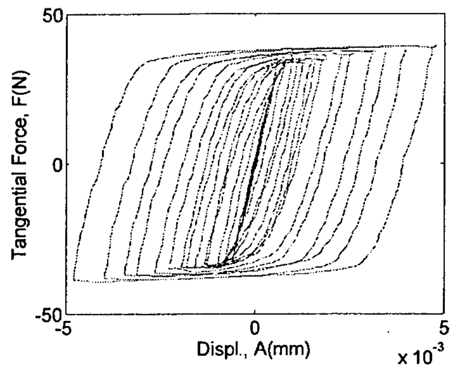

Figure 9: Hysteresis curves from dynamic tests

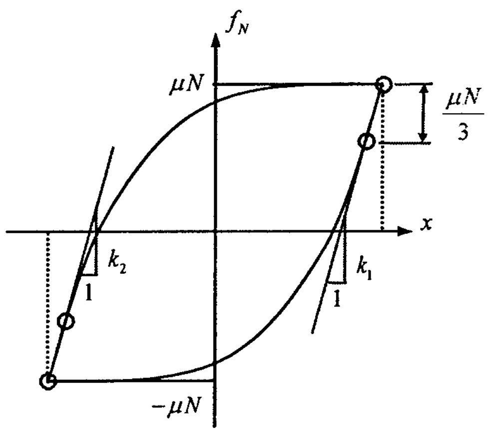

Figure 10: Calculating damper stiffness from the hysteresis

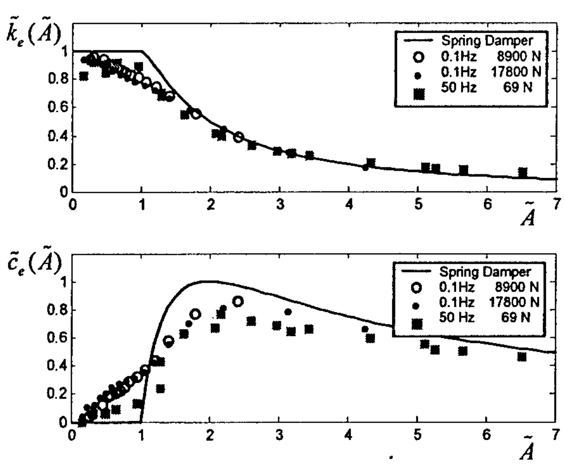

Figure 11: Experimentally generated curves compared with benchmark

The values of damper stiffness determined from the experiments are summarized in Table 1. Note that the stiffness of the quasi-static specimen increased with normal load.

Table 1: Stiffness values from experiments

Dynamic condition (Hz)	Radius (m)	Normal load (N)	$\bar{k}_{Exp}$(N/m)
Dynamic (50)	0.0127	69	$31.6\times10^{6}\,{}^{+11.6\%}_{-7.9\%}$
Quasi-static (0.1)	0.127	8900	$327\times10^{6}\,{}^{+5.0\%}_{-8.2\%}$
Quasi-static (0.1)	0.127	17800	$401\times10^{6}\,{}^{+9.1\%}_{-4.7\%}$

In the next section a classical elasticity solution will be investigated in order to assess the extent to which it captures the behavior seen in the tests.

3. AN ANALYTICAL MODEL: MINDLIN'S APPROXIMATE SOLUTION

In this section an approximate solution by Mindlin [25] is summarized for the elasticity problem of a tangential load applied to a sphere in contact with a half space. It will be used to calculate the damper's stiffness, k_d, the hysteresis curves, and the dimensionless effective stiffness and damping curves for a sphere on a half space.

An interesting aspect of three-dimensional-contact problems in elasticity is that the relative displacement between the contacting bodies approaches a finite limit in the far field. For example, when a sphere contacts the flat surface shown in Figure 12, this behavior limits the relative displacement between the bodies. Thus, when shear loads are applied the displacement of the center line has the behavior indicated by x in Figure 13 provided there is no gross slip.

Consequently, there is a unique stiffness k_∞ that characterizes the far field behavior. From Mindlin's theory the far field stiffness is:

$$k_d \approx k_\infty = \frac{F}{x_\infty} = \left(\frac{4Ga}{2-\nu}\right) = \left(\frac{4G}{2-\nu}\right)\cdot\left[\frac{3NR(1-\nu)}{4G}\right]^{1/3} \tag{7}$$

where G is the shear modulus, ν is Poisson's ratio, R is the radius of curvature, a is the contact radius, and N is the normal load.

Mindlin also gives analytical expressions that define the various parts of the hysteresis curves, Figure 14(a). Specifically, the relative motion is given by:

For the initial loading with zero initial displacement (OPQ in Figure (14))

$$x = \frac{3}{2}A_0\left[1-\left(1-\frac{F}{\mu N}\right)^{2/3}\right] \tag{8}$$

for unloading (PRS in Figure 14))

$$x = \frac{3}{2}A_0\left[2\left(1-\frac{F^*-F}{2\mu N}\right)^{2/3}-\left(1-\frac{F^*}{\mu N}\right)^{2/3}-1\right] \tag{9}$$

and for cyclic reloading (STP in Figure 14)

$$x = -\frac{3}{2}A_0\left[2\left(1-\frac{F^*+F}{2\mu N}\right)^{2/3}-\left(1-\frac{F^*}{\mu N}\right)^{2/3}-1\right] \tag{10}$$

where $A_0 = \frac{\mu N}{k_d}$ (11)

These formulae were used to generate the hysteresis curves shown in Figure 14(b). The curves were processed in the same manner as the experimental data to determine the dimensionless effective stiffness and damping curves for the Mindlin model.

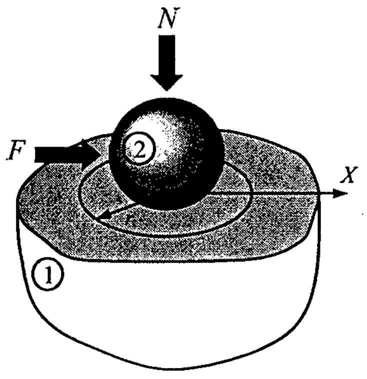

Figure 12: Friction contact of sphere on a flat surface

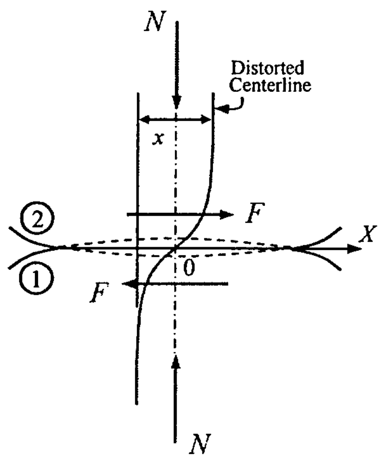

Figure 13: Relative displacement between two bodies in contact ($F < \mu N$)

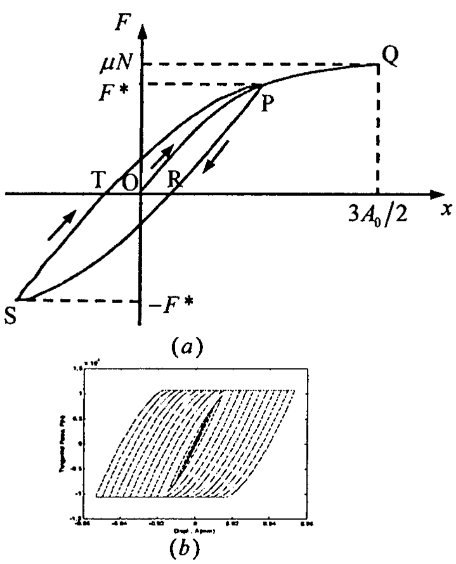

Figure 14: Hysteresis from Mindlin analysis

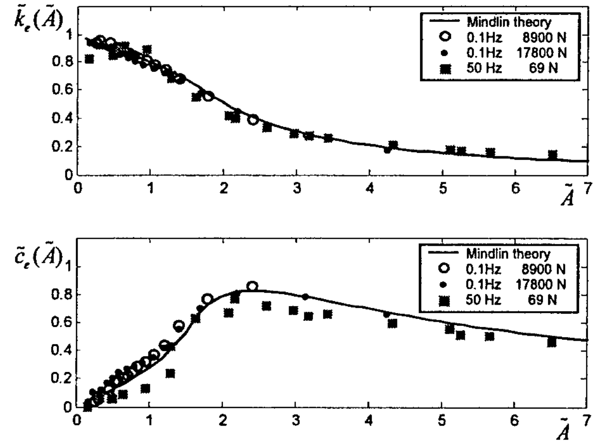

Figure 15: Comparison between experiments and Mindlin analysis

Comparisons between the experimental results and the result from Mindlin's analysis are shown in Figure 15. In general, the agreement is quite good.

Mindlin's estimate of the damper's physical stiffness (7) is a function of material properties, normal load, and radius. A comparison of the stiffnesses measured in the experiment and those calculated from (7) is shown in Table 2. It is clear that Mindlin's formula certainly captures the trend seen in the experiments. This is quite remarkable considering the wide difference in the test conditions in the quasi-static and dynamic tests.

Table 2: Stiffness comparison between experiments and Mindlin theory

Dynamic Condition (Hz)	Radius (m)	Normal load (N)	$\bar{k}_{Exp}$ (N/m)	$k_{Mindlin}$ (N/m)
Dynamic (50)	0.0127	69	$31.6\times10^6 \; {}^{+11.6\%}_{-7.9\%}$	31.7×10^6
Quasi-static (0.1)	0.127	8900	$327\times10^6 \; {}^{+5.0\%}_{-8.2\%}$	345×10^6
Quasi-static (0.1)	0.127	17800	$401\times10^6 \; {}^{+9.1\%}_{-4.7\%}$	435×10^6

4. MODEL IMPLICATIONS

Since the Mindlin analysis agreed well with the experimental data, it was used to examine other implications of the theory. First, rewrite (9) – (11) in dimensionless form where $\tilde{x} \equiv x/A_0$ and $\tilde{f}_N \equiv f_N/\mu N$. Then

$$\tilde{x} = \frac{3}{2}\left[1-\left(1-\tilde{f}_N\right)^{2/3}\right] \quad \text{for OPQ} \qquad (12)$$

At the point P in Figure 16, $\tilde{x} = \tilde{A}$ and $\tilde{f}_N = \tilde{f}_N^*$. Equation (12) implies

$$\tilde{f}_N^* = \tilde{f}_N^*\left(\tilde{A}\right) = 1-\left(1-\frac{2}{3}\tilde{A}\right)^{2/3} \qquad (13)$$

and (10) and (11) imply

$$\tilde{x}=\frac{3}{2}\left[2\left(1-\frac{\tilde{f}_N^{\bullet}-\tilde{f}_N}{2}\right)^{2/3}-\left(1-\tilde{f}_N^{\bullet}\right)^{2/3}-1\right] \quad \text{for PRS} \quad (14)$$

$$\tilde{x}=-\frac{3}{2}\left[2\left(1-\frac{\tilde{f}_N^{\bullet}+\tilde{f}_N}{2}\right)^{2/3}-\left(1-\tilde{f}_N^{\bullet}\right)^{2/3}-1\right] \quad \text{for STP} \quad (15)$$

Inverting (14) and (15) to find explicit expressions for the cyclic force $\tilde{f}_N$ results in

$$\tilde{f}_N\left(\tilde{A},\,\theta\right)=\tilde{f}_N^{\bullet}-2\left\{1-\left(\frac{1}{2}\right)^{3/2}\left[\frac{2}{3}\tilde{A}\cos\theta+\left(1-\tilde{f}_N^{\bullet}\right)^{2/3}+1\right]^{3/2}\right\} \quad (16)$$
for PRS

$$\tilde{f}_N\left(\tilde{A},\,\theta\right)=-\tilde{f}_N^{\bullet}+2\left\{1-\left(\frac{1}{2}\right)^{3/2}\left[-\frac{2}{3}\tilde{A}\cos\theta+\left(1-\tilde{f}_N^{\bullet}\right)^{2/3}+1\right]^{3/2}\right\} \quad (17)$$
for STP

where $\tilde{f}_N^{\bullet}=\tilde{f}_N^{\bullet}\left(\tilde{A}\right)$ is given by (13). Now substitute (16) and (17) into (5) and (6). It is clear that

$$\tilde{k}_e(\tilde{A})=\frac{\frac{1}{\pi}\int_0^{2\pi}\tilde{f}_N\left(\tilde{A},\,\theta\right)\cos\theta d\theta}{\tilde{A}} \quad (18)$$

$$\tilde{c}_e(\tilde{A})=-\frac{\int_0^{2\pi}\tilde{f}_N\left(\tilde{A},\,\theta\right)\sin\theta d\theta}{\tilde{A}} \quad (19)$$

Since the θ dependence in (18) and (19) is integrated out, it is found that the dimensionless effective stiffness and damping are only functions of dimensionless amplitude $\tilde{A}$.

$$\tilde{k}_e(\tilde{A})=\frac{F_c\left(\tilde{A}\right)}{\tilde{A}} \quad (20)$$

$$\tilde{c}_e(\tilde{A})=-\frac{\pi\cdot F_s\left(\tilde{A}\right)}{\tilde{A}} \quad (21)$$

where

$$F_c\left(\tilde{A}\right)\equiv\frac{1}{\pi}\int_0^{2\pi}\tilde{f}_N\left(\tilde{A},\,\theta\right)\cos\theta d\theta \quad (22)$$

$$F_s\left(\tilde{A}\right)\equiv\frac{1}{\pi}\int_0^{2\pi}\tilde{f}_N\left(\tilde{A},\,\theta\right)\sin\theta d\theta \quad (23)$$

Consequently, it is clear that the dimensionless effective stiffness and damping predicted by Mindlin's theory are independent of size, material, normal load, and friction coefficient. Thus, according to Mindlin's theory, there are unique nonlinear, dimensionless stiffness and damping curves for a sphere on a half space.

Another result from Mindlin's theory is that you can determine how the stiffness and damping change for small motions. To first order, the dimensionless, nonlinear stiffness decreases by $\tilde{A}/6$ and the damping equals $2\tilde{A}/9$. In dimensional terms, for example, this means that for physical amplitudes A less than $\mu N/k_d$ the effective damping is approximately equal to

$$c_e(A)=\frac{2A\,k_d^2}{9\omega\pi\mu N} \quad (24)$$

5. CONCLUDING REMARKS

While in general it is not possible to use nondimensionalization techniques for highly non-linear systems, in the case of the spherical damper geometry considered in this paper it was found that the test data and the analytical solution indicate there is a unique set of dimensionless curves that characterize its performance. In addition, two additional parameters, k_d and μ, need to be known in order to complete the description of a specific damper. It was found that the stiffness of the spherical damper k_d could be reasonably well approximated by Mindlin's theory, equation (7). Since Mindlin's theory is based on an elasticity analysis that takes into account nonlinear contact this results suggests that the stiffness of dampers used by industry might be calculated from elasticity theory provided sufficient care is taken to model the effect of nonlinear contact and the resulting, very local stress concentrations.

The harmonic balance method was used to calculate the vibratory response of a frictionally damped, single degree of freedom oscillator in which the friction element was represented by a spring damper [16] and then by the Mindlin model. The results are shown in the damper optimization curves of Figure 17. Damper optimization curves plot the maximum amplitude of response, A_{peak}, as a function of the normal load, N, applied to the friction joint [16]. In most applications, turbine blade dampers are designed to work in the white-colored range. In fact, this range corresponds to the white colored range in Figure 18 where the dimensionless amplitude $\tilde{A}$ varies between 0 and 1.094. In this operating range, it is clear that the real damping was very different from that predicted by the spring model. The results imply that microslip effects may be very important over the part of the operating range typically used by friction damper designers. Based on these observations, it is believed that the problem that the friction damper designers have in calculating the correct damper stiffness is due in part to the fact that their models may not properly account for microslip. As a result, they are changing a parameter in their macroslip model, k_d, in order to try to match behavior that is dominated by microslip effects. This hypothesis that industrial dampers primarily work in the microslip regime is also supported by the fact that industrial dampers rarely show gross wear after use in the engine. However, whenever the test data were taken for $\tilde{A} > 2$, significant levels of wear were observed after only a few hundred cycles.

Lastly, an additional challenge remains in predicting the coefficient of friction, μ. During the experiments it was observed that μ changed with time as the surface finish of the

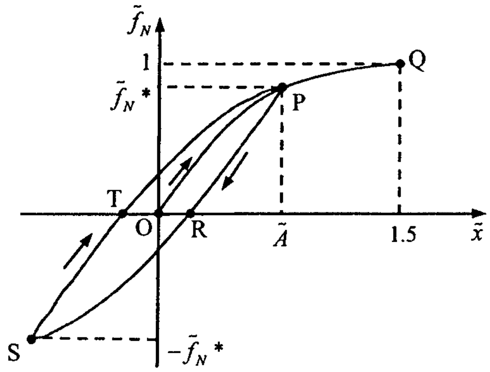

Figure 16: Dimensionless hysteresis loop from Mindlin theory

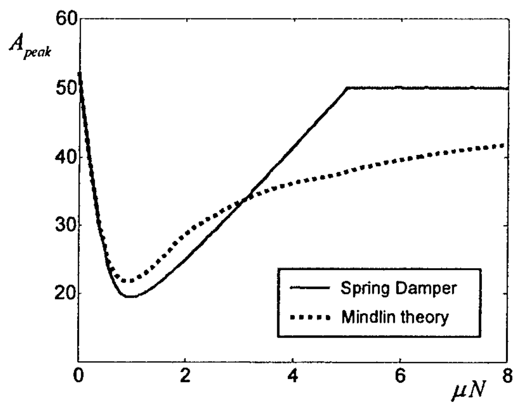

Figure 17: Design range in damper optimization curve

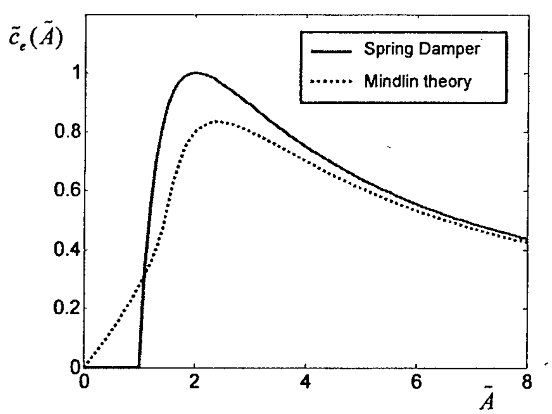

Figure 18: Design range in effective damping curve

contact surfaces degraded.[2] Consequently, it is an open issue what its value would be after the damper has operated for some time in the engine. In our tests μ increased by about a factor of two when the motion across the friction interface became large after enough cycles. If the damper does, in fact, work in the microslip regime, then from (24) it is clear that an increase in μ would result in less damping and higher vibratory response. Consequently, it is important to insure that μ achieves a stable value representative of engine operating conditions in evaluating the damper's effectiveness during early testing.

[2] Note that we had to periodically measure μ and take its change into account in developing the dimensionless damping and stiffness curves quoted in this paper.

ACKNOWLEDGMENTS

This research was supported by NAVAIR, contract number N00421-01-1-0001 and by AFOSR, award number F49620-02-1-0168. The authors would like to acknowledge the stimulating discussions and suggestions provided by Dr. Daniel J. Segalman of Sandia National Laboratories.

REFERENCES

[1] Feeny, B.F., Guran, A., Hinrichs, N., and Popp, K., 1998, "A Historical Review of Dry Friction and Stick-Slip Phenomena," *Applied Mechanics Reviews*, Vol. 51, No. 5, pp. 321-341.

[2] Gaul, L. and Nitsche, R., 2001, "The Role of Friction in Mechanical Joints," *Applied Mechanics Reviews*, Vol. 54, No. 2, pp. 93-106.

[3] Griffin, J.H., 1990, "A Review of Friction Damping of Turbine Blade Vibration," *International Journal of Turbo and Jet Engines*, Vol. 7, pp. 297-307.

[4] Yang, B.D. and Menq, C.H., 1997, "Modeling of Friction Contact and Its Application to the Design of Shroud Contact," *ASME Journal of Engineering for Gas Turbines and Power*, Vol. 119, No. 4, pp. 958-963.

[5] Yang, B.D. and Menq, C.H., 1998, "Characterization of Contact Kinematics and Application to the Design of Wedge Dampers in Turbomachinery Blading, Part I: Stick-slip Contact Kinematics," *ASME Journal of Engineering for Gas Turbines and Power*, Vol. 120, No. 2, pp. 410-417.

[6] Yang, B.D. and Menq, C.H., 1998, "Characterization of Contact Kinematics and Application to the Design of Wedge Dampers in Turbomachinery Blading, Part II: Prediction of Forced Response and Experimental Verification," *ASME Journal of Engineering for Gas Turbines and Power*, Vol. 120, No. 2, pp. 418-423.

[7] Yang, B.D. and Menq, C.H., 1998, "Characterization of 3D Contact Kinematics and Prediction of Resonant Response of Structures Having 3D Frictional Constraint," *Journal of Sound and Vibration*, Vol. 217, No. 5, pp. 909-925.

[8] Sanliturk, K.Y., Ewins, D.J. and Stanbridge, A.B., 2001, "Underplatform Dampers for Turbine Blades: Theoretical Modeling, Analysis and Comparison with Experimental Data," *ASME Journal of Engineering for Gas Turbine and Power*, Vol. 123, pp. 919-929.

[9] Petrov, E.P., Ewins, D.J., 2003, "Analytical Formulation of Friction Interface Elements for Analysis on Nonlinear Multi-Harmonic Vibrations of Bladed Discs," *ASME*

Journal of Turbomachinery, Vol. 125, pp. 364-371.

[10] Petrov, E. P. and Ewins, D.J., 2003, "Generic Friction Models for Time-domain Vibration Analysis of Bladed Discs," *Proceedings of ASME Turbo Expo 2003, Atlanta, Georgia*, GT-2003-38475.

[11] Szwedowicz, J., Kissel, M., Ravindra, B., and Kellerer, R., 2001, "Estimation of contact stiffness and its role in the design of a friction damper," *Proceedings of ASME Turbo Expo*, 2001-GT-0290.

[12] Cha, D. and Sinha, A., 1999, "Computation of the Optimal Normal Load of a Friction Damper under Different Types of Excitation," *ASME International Gas Turbine Conference, Indianapolis, IN*, ASME 99-GT-413.

[13] Cha, D. and Sinha, A., 2000, "Statistics of Responses of a Mistuned and Frictionally Damped Bladed Disk Assembly Subjected to White Noise and Narrow Band Excitations," *ASME International Gas Turbine Conference, Munich, Germany*, ASME 2000-GT-542.

[14] Csaba, G., 1999, "Modeling of a Microslip Friction Damper Subjected to Translation and Rotation," *ASME International Gas Turbine Conference, Indianapolis, IN*, ASME 99-GT-149.

[15] Sextro, W., Popp, K., and Wolter, I., 1997, "Improved Reliability of Bladed Disks Due to Friction Dampers," *ASME International Gas Turbine Conference*, ASME 97-GT-189.

[16] Griffin, J.H., 1980, "Friction Damping of Resonant Stresses in Gas Turbine Engine Airfoils," *ASME Journal of Engineering for Power*, Vol. 102, pp. 329-333.

[17] Menq, C.H., Griffin, J.H. and Bielak, J., 1986, "The Influence of a Variable Normal Load on the Forced Vibration of a Frictionally Damped Structure," *ASME Journal of Engineering for Gas Turbines and Power*, Vol. 108, pp. 300-305.

[18] Yang, B.D., Chu, M.L. and Menq, C.H., 1998, "Stick-slip-separation Analysis and Nonlinear Stiffness and Damping Characterization of Friction Contacts Having Variable Normal Load," *Journal of Sound and Vibration*, Vol. 210, No. 4, pp. 461-481.

[19] Menq, C.H., Chidamparam, P. and Griffin, J.H., 1991, "Friction Damping of Two-dimensional Motion and Its Application in Vibration Control," *Journal of Sound and Vibration*, Vol. 144, pp. 427-447.

[20] Menq, C.H. and Yang, B.D., 1998 "Nonlinear Spring Resistance and Friction Damping of Frictional Constraint Having Two Dimensional Motion," *Journal of Sound and Vibration*, Vol. 217, No. 1, pp. 127-143.

[21] Ewins, D.J. and Griffin, J.H., 2001, "Workshop on the Modeling, Analysis, and Measurement of Friction Constraints in Gas Turbine Components," *Final Report submitted to USAF, AFRL, AFOSR/NA*, Award Number: F49620-01-1-0325.

[22] Mindlin, R.D., 1949, "Compliance of Elastic Bodies in Contact," *Journal of Applied Mechanics*, Vol. 16, pp. 259-268.

[23] Mindlin, R.D., Deresiewicz, H., 1953, "Elastic Spheres in Contact Under Varying Oblique Forces," *Journal of Applied Mechanics*, Vol. 20, pp. 327-343.

[24] Deresiewicz, H., 1957, "Oblique Contact of Non-Spherical Bodies," *Journal of Applied Mechanics*, Vol. 24, pp. 623.

[25] Mindlin, R.D., Mason, W.P., Osmer, T.F., and Deresiewicz, H., 1952, "Effects of an Oscillating Tangential Force on the Contact Surfaces of Elastic Spheres," *Proceedings of the First U. S. National Congress of Applied Mechanics*, pp. 203-208.

[26] Johnson, K. L., 1955, "Surface Interaction between Elastically Loaded Bodies under Tangential Forces," *Proceedings Royal Society*, A230, pp. 531-549.

[27] Goodman, L.E., and Brown, C.B., 1962, "Energy Dissipation in Contact Friction: Constant Normal and Cyclic Tangential Loading," *Journal of Applied Mechanics*, Vol. 29, pp. 17-22.

[28] J.P. Den Hartog, 1931, "Forced Vibrations with Combined Coulomb and Viscous Friction," *Tansactions of the ASME*, Vol. 53, pp. 107-115.

[29] T.K. Caughey, 1960, "Sinusoidal Excitation of a System with Bilinear Hysteresis," *ASME Journal of Applied Mechanics*, Vol. 27, pp. 640-643.

[30] L. Gaul, 1983, "Wave Transmission and Energy Dissipation at Structural and Machine Joints," *ASME Journal of Vibration, Acoustics, Stress and Reliability in Design*, Vol. 105, pp. 489-496.

[31] Meng, C.H., Griffin, J.H., 1985 "A Comparison of Transient and Steady State Finite Element Analyses of the Forced Response of a Frictionally Damped Beam," *ASME Journal of Vibration, Acoustics, Stress, and Reliability in Design*, Vol. 107, pp. 19-25.

[32] Filippi, S., Akay, A. and Gola, M.M., 2003, "Measurement of Tangential Contact Hysteresis During Microslip," submitted to the *ASME Journal of Tribology*.